Crystalline to amorphous transition and band structure evolution in ion-damaged silicon studied by spectroscopic ellipsometry

P. K. Giri,[a] S. Tripurasundari, G. Raghavan, B. K. Panigrahi, P. Magudapathy, K. G. M. Nair, and A. K. Tyagi
Materials Science Division, Indira Gandhi Centre For Atomic Research, Kalpakkam-603102, India

Crystalline to amorphous transition and subsequent microstructural evolution in silicon induced by Ar^+-ion implantation over a wide range of ion fluences (6×10^{13}–1×10^{17} cm^{-2}) have been investigated by spectroscopic ellipsometry. In the evaluation of the optical and microstructural properties of the damaged layer, the contribution of the surface overlayer to the measured dielectric spectra was separated by fitting a multilayer model with an effective medium approximation. The best fit to the dielectric spectra for disordered silicon could be obtained by taking our highest-fluence implanted (fluence=1×10^{17} ions/cm^2) amorphous silicon (*a*-Si) data as reference data instead of *a*-Si data available in the handbook. The derivative spectra as a function of fluence show a distinct and sharp transition from the crystalline to amorphous phase. The threshold fluence for this transition is derived from fitting. Evaluation of standard sum rules and optical moments for imaginary part of the pseudodielectric function reveals no substantial change in various physical parameters below the transition indicating their insensitivity to point defects, while it shows a large change with fluence above the threshold for amorphization. The disorder induced changes in the effective dielectric constant, number of valence electrons per atom participating in optical transition, Penn gap energy, average bond length, coordination number, effective dispersion oscillator energy, an average strength of the interband optical transition with fluence is discussed on the basis of microstructural evolution and corresponding band structure modification. It is also shown that the dielectric functions of damaged silicon are well represented by a sum of six classical Lorentz oscillators. With increasing fluences, each of the oscillator amplitude decreases and linewidth increases except for the 3.3 eV transition which shows increasing amplitude with fluence. These results are discussed in the context of short-range order/disorder and effective band gap reduction along with flattening of the bands with increasing fluence above the amorphization threshold. © *2001 American Institute of Physics.* [DOI: 10.1063/1.1379055]

I. INTRODUCTION

Ion-beam induced changes in optical and electronic properties of a semiconductor have been a subject of intense research due to its technological importance as well as fundamental interest, particularly in studies of the crystalline to amorphous (*c*-*a*) transition induced by energetic heavy ions.[1–5] Ion implantation provides a convenient means to tailor the material properties and it can provide significant insights into the relationship between electronic properties and solid structure. By a suitable choice of implantation parameters, it is possible to obtain material properties continuously varying from crystalline to amorphous structure. A number of experimental tools such as Rutherford backscattering spectrometry (RBS),[6] transmission electron microscopy (TEM),[7] x-ray diffraction,[8] Raman scattering,[9] optical reflectivity,[10] ellipsometry,[11] and modulation technique,[12] with a varying degree of sensitivity, have been utilized in the past to understand the process of disorder and related effects in crystalline material. A large number of studies have been devoted to understand the process of amorphization due to implantation in semiconductors, and primarily two models

for amorphization have been suggested in the literature. In the homogeneous amorphization model, amorphization is thought to be a phase transition induced by the accumulation of a sufficient number of defects in crystalline Si. On the other hand, in the heterogeneous amorphization model, the continuous amorphous layer is believed to form due to a sufficient overlap of the amorphized cylindrical cascades. A nucleation-and-growth character of the *c*-*a* transition in accordance with the homogeneous model was clearly established by Rault *et al.* using *in situ* TEM analysis and the heterogeneous nucleation model for amorphization was ruled out.[13] More recently, the defect induced nucleation and growth of amorphous Si (*a*-Si) has been proposed[14] and it provides a view to comprehend different aspects of the homogeneous amorphization model. In several studies, the implantation-induced amorphization process has been viewed as a critical-point phenomena consisting of cooperative processes[1,2] and a sharp transition has been observed in some studies,[2] contrary to the picture of gradual buildup of damage leading to the amorphization beyond a certain number of displacements per atom (DPA).

In spite of the large number of studies on amorphous Si (*a*-Si), a detailed understanding on the microscopic structure of pure *a*-Si remains unclear.[15,16] The optical properties of

[a]Electronic mail: pkgiri@igcar.ernet.in

a-Si prepared by conventional deposition techniques (*d*-*a*-Si), such as glow discharge, have been extensively studied in the literature and are known to be strongly dependent on the details of the growth conditions.[17] On the other hand, the properties of disordered and pure amorphous silicon produced by ion irradiation (*i*-*a*-Si) are relatively less understood. A continuous random network (CRN) model[18] has been widely accepted to account for the observed electronic and optical properties of *d*-*a*-Si, while *i*-*a*-Si seems to differ in local structures such as medium- and short-range order as evidenced from recent x-ray scattering studies.[8,16] A microcrystalline model seems to be more appropriate for description of the geometrical structure of *i*-*a*-Si. Recent studies using fluctuation microscopy showed that ion-implanted *a*-Si has more medium-range order than expected from the CRN model[19] and the structure can be described as paracrystalline, i.e., it possesses crystalline-like order which decays with distance from any point.[19,20] It has also been shown that the conventionally used radial distribution function (RDF) is very insensitive to medium-range order and is inadequate for exact evaluation of microstructure of *i*-*a*-Si.[19] It is well established that *d*-*a*-Si contains a substantial amount of voids, whereas *i*-*a*-Si does not contain any void,[21] while it may be saturated with small clusters of vacancies and interstitials.[14] In *a*-Si:H, the dominant defects are found to be dangling bonds, whereas in pure *a*-Si several other kinds of defects have been observed.[22] Hence, a systematic study on microstructure and related optical properties of *i*-*a*-Si is necessary to understand the role of short-range order/disorder in determining the properties of pure amorphous Si.

The complex dielectric function $\varepsilon(E) = \varepsilon_1(E) + i\varepsilon_2(E)$ is known to describe the optical properties of the medium at photon energy $E = \hbar\omega$. Among various optical techniques, spectroscopic ellipsometry is an extremely sensitive and powerful tool to evaluate spectral dependence of $\varepsilon(E)$ and can provide important information on electronic band structure and microstructural changes induced by ion damage. In the past, spectroscopic ellipsometry has been extensively used for nondestructive depth profiling and characterization of multilayer structures and interfaces with considerable success.[23] For crystalline silicon (*c*-Si), the optical spectra show characteristic sharp features near the critical points (CP).[24] With lattice disorder induced by ion implantation at sufficiently high fluences, crystal periodicity is lost and the sharp optical features are altered,[25] becoming almost structureless if the implanted region turns completely amorphous. A large number of investigations have been made using ellipsometry on the microstructure of the damaged layers and the damage depth profile[26,27] produced by ion implantation. Though the ion-damaged layer is often modeled as a mixture of *c*-Si and *a*-Si in the effective medium approximation (EMA), it has been recognized that the complex dielectric function of implanted *a*-Si differs from that of annealed (relaxed) *a*-Si as well as from that of evaporated *a*-Si.[28] However, related microscopic parameters responsible for such differences are not understood properly. It would be interesting to study the changes in various physical parameters such as density of free carriers, effective dielectric constant, Penn gap, dispersion energy, and strength of the oscillator related

to the optical transition in order to understand the continuous evolution of the system with increasing disorder. Furthermore, studies on the modification of the band structure with controlled disorder would be insightful in exploiting these materials for optoelectronic applications.

In this work, we have used spectroscopic ellipsometry to investigate the nature of crystalline to amorphous transition and microstructural evolution in silicon as a function of fluence spanning over four orders of magnitude. Particular attention was paid to remove the contribution of the oxide overlayer from the measured dielectric spectra by fitting a multilayer model using the EMA and corrected spectra are used for all subsequent analysis. This correction has important bearing on the extracted parameters from the dielectric spectra, as the strong effect of the oxide overlayer on dielectric spectra measured by ellipsometry have been recognized in the past.[29] The systematic evolution of optical spectra with increasing ion fluence is analyzed using the difference spectra. A sharp transition in dielectric spectra is observed beyond threshold fluence corresponding to crystalline to amorphous transition and threshold for amorphization is obtained from fitting of derivative spectra. Various moments of $\varepsilon_2(E)$ are evaluated to get an insight into the local structures and modification of the band structure in defected Si and pure *a*-Si. The changes in the amplitude and linewidth of the principal optical transitions with fluence were evaluated by fitting a finite number of Lorentz oscillators. These results are discussed in the context of medium-range and short-range order/disorder model and band structure modification.

II. EXPERIMENTAL DETAILS

We used Czochralski grown boron doped polished Si(100) wafers for the present study. The Ar$^+$-ion implantations were performed at room temperature with energy 120 keV and at fluences in the range $6 \times 10^{13} - 1 \times 10^{17}$ ions/cm^2. The samples were implanted at normal incidence using a 150 keV ion accelerator. The beam current was maintained low enough (~500 nA) not to cause any substantial heating of samples during implantation. The Si wafers were degreased with trichloroethelene, acetone, and methanol sequentially before and after the implantation. Spectroscopic ellipsometry measurements were performed with a rotating polarizer type ellipsometer (SOPRA model ESVG4) in the photon energy range 0.6–5 eV for a fixed angle (75°) of incidence.

III. THEORETICAL CONSIDERATIONS

A. General sum rules and moment relationships: The Penn model and other parameterization schemes

The well-known sum rules and the optical moments of the dielectric function $\varepsilon(E)$ provide useful insight into the nature of the electronic structure. We have evaluated these quantities from our experimental results because of the following reasons. (i) The moments in the disordered system reflect the average properties of the electronic structure rather than the detailed properties of particular eigenstates, and (ii) a direct comparison of the moments for differently disordered samples provides a more meaningful basis for the discussion of the differences between materials with similar

short-range order. They also provide insight into the band-structure modification, subtle differences in bonding between amorphous and crystalline semiconductors and the nature of the $c-a$ transition.

Optical moment M_r of the $\varepsilon_2(E)$ is related to the macroscopic quantities like effective dielectric constant ($\varepsilon_{0,\text{eff}}$), effective number of valence electrons (n_{eff}) through the relationship[30]

$$\varepsilon_{0,\text{eff}} = 1 + M_{-1}, \tag{1}$$

$$n_{\text{eff}} = (m/4\pi e^2 N) M_1, \tag{2}$$

where

$$M_r = \frac{2}{\pi} \int_{E_g}^{\infty} E^r \varepsilon_2(E) dE. \tag{3}$$

These integral relationships do not depend on the details of the line shape of $\varepsilon_2(E)$ and on the presence or absence of critical points. Hence, they are particularly useful for the comparison of materials containing different degrees of disorder. The earlier quantities are calculated up to a maximum energy 5.0 eV, used in this work. Although higher energy data may contribute to the evaluation of the integrals, the present results are believed to be highly suggestive of the nature of changes occurring with increasing disorder.

The Penn gap energy E_g is defined through the expression[31]

$$E_g^2 = M_1 / M_{-1}, \tag{4}$$

that represents the average separation between bonding and antibonding states. Equation (4) represents a single oscillator approximation to the dielectric response of the solid. The Penn gap E_g plays the pivotal role in the theory of ionicity due to Phillips and van Vechten,[32] where it is a measure of the average bond strength that can be sensibly divided into a covalent and an ionic contribution, and in a good approximation this energy coincides with the maximum of $\varepsilon_2(E)$ spectrum in a-Si. In this case, disorder induced change in E_g is used as a monitor for degree of covalency retained in damaged Si.

Introduced by Wemple and DiDomenico,[33] the oscillator strength E_0 defined through

$$E_0^2 = M_{-1} / M_{-3} \tag{5}$$

takes the place of E_g. The definition of E_g and E_0 as ratios of two moments of $\varepsilon_2(E)$ of equal power makes these quantities independent of the amplitude of $\varepsilon_2(E)$ which is determined by the magnitude of the transition matrix element. The second energy E_d is defined as[33]

$$E_d^2 = M_{-1}^3 / M_{-3} \tag{6}$$

takes such variations in the oscillator strength of interband transitions into account. It should be noted that E_d is dependent on the magnitude of $\varepsilon_2(E)$ in contrast to E_g which does not, so that interband transition strengths are not contained in E_g.

B. Harmonic oscillator approximation

The dielectric function of a real solid can often be adequately reproduced by a sum over a finite number of classical Lorentz oscillators, expressed as[34]

$$\varepsilon(E) = 1 + \sum_{i=1}^{n} \left(\frac{\eta \omega_{p,i}}{2E_i} \right)^2 \left(\frac{1}{E + E_i + i\Gamma_i} - \frac{1}{E - E_i + i\Gamma_i} \right), \tag{7}$$

where E_i and Γ_i are the energy and broadening parameter of the ith oscillator, and ω_p is the plasmon frequency. The first term in the sum represents the amplitude (A_i) of the individual oscillator. Though Eq. (7) is a simplified form of a more general expression containing an integration on momentum matrix element over the Brillouin zone, it can be well represented by the summation over a finite number of oscillators which are weakly coupled and can be grouped by critical points to reduce the total numbers needed to represent a real spectrum. We use the earlier approximation to evaluate the effect of increasing disorder on the amplitude and broadening of each oscillator and discuss the relevant modifications in the band structure.

IV. RESULTS AND DISCUSSION

The ellipsometric measurements were made for the energy range 0.6–5.0 eV for an incidence angle of 75°. Measurements in the infrared region of the incident light show small peak structures and oscillations in the dielectric spectra, primarily related to the interference at the amorphous-crystalline a-c interface and due to the finite thickness of the a-Si layer compared to the penetration depth of light at these wavelengths. The low energy peaks in the dielectric spectra become more prominent with increasing fluence above the amorphization threshold and it is attributed to the sharpening of the a-c interface.[35] However, they do not contain any significant information on the microstructural changes in damaged layer. Hence, we use the dielectric spectra in the energy range 1.5–5.0 eV, for all subsequent analysis.

In crystalline Si, the complex dielectric spectrum $\varepsilon(E) = \varepsilon_1(E) + i\varepsilon_2(E)$ is known to be dominated by two major peaks usually denoted by E_1 and E_2. In the ε_2 spectrum of the virgin sample, we noted that the relative amplitude of the E_2 peak is less than the E_1 peak, which is in contrast to that expected for single crystalline Si.[24] From a linear regression analysis, it became evident that such modification in the spectra is caused by the presence of the native oxide layer on the Si surface. A native oxide layer of about 2–3 nm is known to be present for the silicon surface unless special care is taken to maintain the sample in an inert environment subsequent to etching. Since the present measurements were performed in air ambient, in order to extract the thickness of the oxide layer in each sample, we used a multilayer model to fit the experimental data. EMA was used to model the damaged Si layer as a mixture of crystalline (c-Si), polycrystalline (poly-Si) and amorphous (a-Si) layers. For the ion-damaged layer, we considered a five-layer model consisting of substrate (c-Si)/layer 2/layer 1/SiO$_2$/ambient (air) as shown in Fig. 1. Here the damaged layers are considered discrete inhomogeneous layers (layer 1 and layer 2) with

Ambient (air)

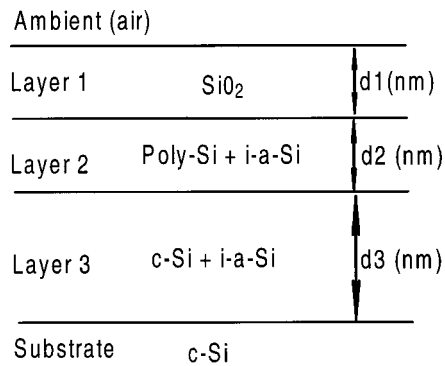| Layer 1 | SiO$_2$ | d1(nm) |
| Layer 2 | Poly-Si + i-a-Si | d2 (nm) |
| Layer 3 | c-Si + i-a-Si | d3 (nm) |

Substrate   c-Si

FIG. 1. Schematic diagram of the multilayer structure used in the linear regression analysis with an effective medium approximation for the fitting of the dielectric spectra from ion-damaged Si.
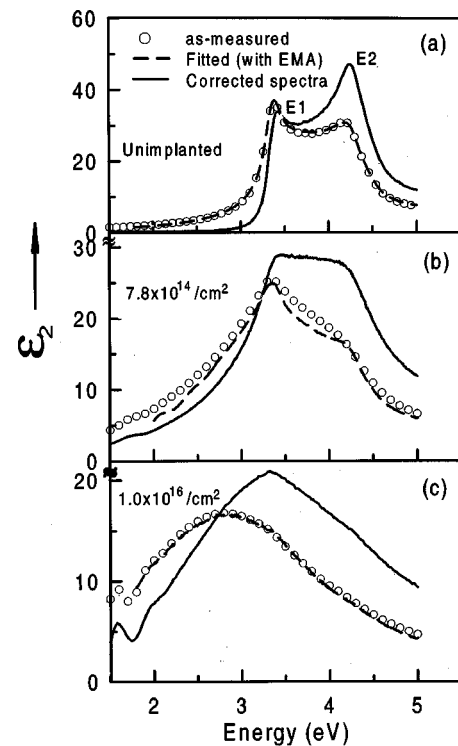
FIG. 2. Imaginary part of the pseudodielectric functions of Ar$^+$ implanted (120 keV at various fluences) silicon: as-measured (open circle), fitting (dashed line) with multilayer model of Fig. 1, and after correction (solid line) of the oxide overlayer.

different proportions of *c*-Si, *a*-Si, and poly-Si. A best fit to the experimental data could be obtained when layer 1 was assumed to consist of mixture of poly-Si and *i-a*-Si, and layer 2 consisting of mixture of *i-a*-Si and *c*-Si. In each case, by the linear regression method, the thicknesses of different layers and the volume fraction of each component in a layer was determined. It is important to mention that a better fit to the experimental data could be obtained by using our own reference sample as the *i-a*-Si, which was obtained by Ar$^+$ implantation at very high fluence (1×10^{17} cm^{-2}). In the reference data, contribution from the oxide layer was stripped-off from the measured spectra to obtain proper data for *i-a*-Si. The regression analysis on the high fluence (1×10^{17} cm^{-2}) sample shows a relatively large thickness of the overlayer, which could be fitted with a mixture of SiO$_2$ and *i-a*-Si. The presence of *i-a*-Si on the surface is likely to be caused by the migration of displaced Si atoms towards the surface, as has been recently observed using RBS and ellipsometry studies.[36] For fitting of spectra for the remaining samples, if we use the data usually found in the handbook for *a*-Si,[37] the fit was found to be poor. This indicates that the dielectric function for pure *i-a*-Si and *d-a*-Si (made by the deposition technique) is different due to distinct differences in their microstructures. Our results are consistent with previous reports.[28] Hence, we use the corrected dielectric function of our highest fluence (1×10^{17} cm^{-2}) sample as the reference sample for *i-a*-Si. This approach was found to give best fits with least standard deviation ($\sigma \sim 0.002$) and a similar approach was adopted by Lee *et al.*[38] in the microstructural modeling of implanted Si.

Note that no inclusion of the void was required in the microstructural modeling of the ion-damaged layer, in contrast to the report by Adachi *et al.*[39] who found a large fraction ($\sim 8.8\%$) of the void in the *i-a*-Si from regression analysis. Our results are consistent with the recent finding that *i-a*-Si does not contain any detectable void compared to *d-a*-Si.[21] Our regression analysis shows a damage depth of ~ 235 nm, which is comparable to the value predicted from TRIM calculation.[40] We find that the thickness of the oxide layer increases with increasing ion fluence, reaching a value of ~ 8.5 nm for fluence 1×10^{16} cm^{-2}, compared to the minimum of ~ 3.2 nm in the case of the virgin Si sample. This may be attributed to the local heating effect during ir-

radiation that results in the growth of an excess oxide layer. Hence, subtracting the contribution of the oxide layer is essential for proper evaluation of the dielectric function. With increasing fluence, the fraction of *i-a*-Si in both layer 1 and layer 2 increases and two layers overlap for larger fluence.

The sharp features related to critical points in the dielectric spectra of *c*-Si gradually diminish with increasing fluence. To obtain the spectra for the ion-damaged layer alone, the contribution from oxide layers to ε_1 and ε_2 are subtracted from the measured spectrum. Figure 2 shows a selection of the ε_2 spectra for three different samples implanted with different fluences; open circles represent the as-measured spectra, the dashed line represents a fitting with the multilayer model, and the solid line represents the data obtained after oxide-layer correction. It may be noted that the multilayer model fitting for low-fluence and high-fluence samples shows better fitting compared to intermediate fluence samples. This implies that samples implanted with fluence near or above the amorphization threshold cannot be well represented by a simple mixture of *a*-Si and *c*-Si, as is assumed in the effective medium approximation. In this approximation, a heterogeneous mixture of *c*-Si and *a*-Si is assumed to represent the characteristics of the damaged layer, which may be inadequate because of the fact that crystalline and amorphous phases are thermodynamically two distinct states. Hence, the inadequate fitting in the present case points towards the need for a homogeneous model to describe the process of the amorphization and the heterogeneous model is less likely. Nevertheless, we use this fitting procedure to estimate the thickness of the oxide layer with
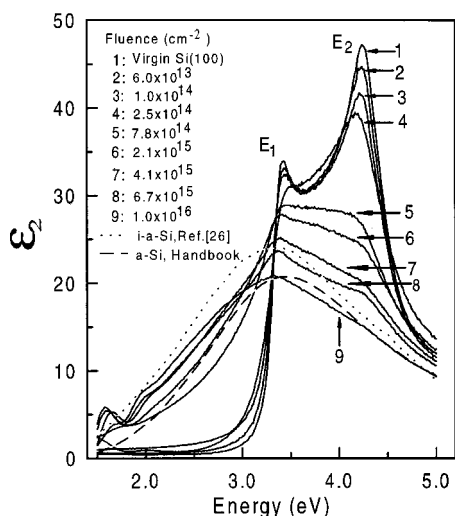
FIG. 3. Imaginary part of the dielectric function for Si samples implanted with various fluences in the range $6 \times 10^{13} - 1 \times 10^{16}$ ions/cm^2. For comparison with our i-a-Si data, spectra for the i-a-Si sample used in Ref. 26 and a-Si data from the handbook (see Ref. 37) are also included.

reasonable accuracy and the corresponding spectrum is subtracted from the measured dielectric spectrum. Two features are notable in Fig. 2 when comparing the as-measured and corrected spectra; (i) relative change of the amplitude of the E_1 and E_2 peaks after correction, and (ii) relative shift of the E_1 peak position and the overall envelope with respect to the spectrum for c-Si, particularly in the case of samples implanted with high fluences. Figure 2(c) shows that the large redshift of the envelope in as-measured spectrum is not characteristic of the damaged layer, but caused by the oxide overlayer on the damaged crystal, which is confirmed from fitting. Hence, the large shift in the E_1 peak position in heavily damaged Si is an artifact due to surface modification by oxidation. Further, the broad feature in the as-measured ε_2 spectrum becomes relatively sharper after correction. Though the effect of overlayers on ellipsometric measurements has been realized from earlier studies, in some studies such effects have been neglected presuming its effect to be small.[41] However, we found that such a correction is essential in high-fluence implanted samples for proper evaluation of the dielectric function. The small redshift ($\sim$0.1 eV) of the corrected E_1 peak envelope seen in Fig. 2(c) can be explained on the basis of the weakening of the covalent bonds due to perturbation created by ion damage. With increasing disorder, the ε_2 spectrum is expected to shift to the lower energies by reducing the splitting between the bonding and the antibonding states.

In Fig. 3 we show a series of ε_2 spectra (corrected) for samples implanted with various fluences in the range $6 \times 10^{13} - 1 \times 10^{16}$ ions/cm^2. For comparison with the samples implanted with high fluences, spectra for ion-beam produced a-Si sample used in Ref. 26 and a-Si data from the handbook[37] are also shown. With increasing fluence, the sharp peaks E_1 and E_2 tend to smear out due to ion-induced disorder in the crystalline Si structure. A drastic drop in the amplitude of the E_2 peak corresponding to the fluence 7.8×10^{14} cm^{-2} indicates the presence of the amorphous layer.

Microstructural fitting for this sample using the EMA showed that the damaged layer consists of about 60% amorphous and $\sim$40% crystalline silicon, besides a thin amorphous layer near the surface. This marked effect of disorder on the E_2 peak compared to the E_1 peak, arises due to the fact that E_2 arises from the transitions in the [100] directions and consequently sensitive to the details of the connectivity of the molecular units in crystalline Si. On the other hand, E_1 arises from the transitions in the [111] directions and these directions being coincident with the direction of bonds within the tetrahedral units of the crystal are expected not to destroy the E_1 peak as it may leave some molecular unit undamaged. It can be noted that the broad peak of ε_2 for our i-a-Si lies close to that of the original E_1 peak of c-Si, and this peak, with small differences, resembles the spectra from a-Si prepared by different methods in terms of its broad feature and mean peak position. However, the minor differences between different amorphous samples can be attributed to the differences in their short-range order. The presence of a detectable peak structure in our i-a-Si sample indicates that not only a short range-order is present in the sample, but also a paracrystalline nature of the medium to some extent.[20] This is in contrast to the case of d-a-Si where the loss of both short-range and long-rage order is responsible for the complete absence of features in the spectra. The difference between amorphous Si prepared by different methods has been reported earlier and is known to depend on the details of the growth conditions. It suffices here to say that the i-a-Si is microscopically different from d-a-Si due to differences in defect structures, local inhomogeneities in structures, bond topology, etc. In ion damaged Si, for intermediate fluence the medium is usually thought to be a mixture of microcrystalline and amorphous pockets. The microcrystallite size reduces with increasing fluence above the amorphization threshold and a small peak-like feature in the ε_2 spectrum is caused by residual small microcrystallites in the disordered region. A similar conclusion has been made from studies on heavily damaged Si, where electroreflectance measurements showed measurable signal due to presence of small crystal grains, though RBS studies indicated complete amorphization of surface layer.[42] Our observation is fully consistent with the recent report on ion-implanted amorphous Si, which showed the presence of medium-range order[19] than is expected from the CRN model. In earlier reports on the dielectric spectra of pure a-Si, a complete absence of sharp features in some studies may be related to the presence of a thin overlayer on the damaged layer which would suppress the sharp spectral features.

A. *c-a* transition

The degree of disorder in crystalline Si has a marked influence on the amplitude of the CP transitions in the ε_2 spectra. In Fig. 4, we show a semilogarithmic plot of the measured peak height (ε_2) as a function of fluence for two major transitions E_1 and E_2. We use the ε_2 value of the fully amorphized sample as a base line and plot the difference $\Delta\varepsilon_2$. The variation is found to be exponential and the plotted data in semilogarithmic scale clearly show two distinct slopes fitted with straight lines (dotted or dashed lines) for
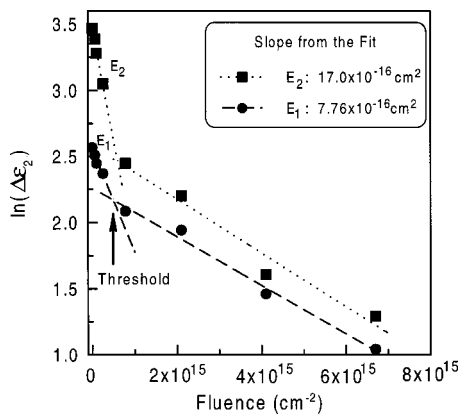
FIG. 4. A semilogarithmic plot of the differential peak heights (in the ε_2 spectra) as a function of fluence for two major transitions E_1 and E_2 showing a drastic change in slope at fluence $\sim 5 \times 10^{14}$ cm^{-2}, pointed with an arrow. The peak value of ε_2 for the fully amorphized sample is used as a base line for calculating the difference $\Delta \varepsilon_2$.

FIG. 5. (a) 3JDOS derivatives of the ε_1 spectra for the Si crystal damaged with 120 keV Ar$^+$ ions at various fluences. (b) Plot of the measured peak-to-peak heights of 3JDOS (E_1, E_2) as a function of the fluence showing two distinct slopes for regions I and II.

the entire fluence range. The presence of two distinct slopes indicates the onset of a transition. This transition refers to a phase transition from the crystalline to amorphous state, where the amorphous state is characterized by a higher free energy and a short-range order in structure. Ion damage causes loss of long-range order and the system evolves from medium-range order to short-range order with increasing fluence. From the crossover point (shown with arrow in Fig. 4) of the two fitted lines, we calculate the threshold fluence for this transition. By solving the simultaneous equations fitted for two regions, we calculated a threshold fluence of $\sim 4.9 \times 10^{14}$ cm^{-2} from the curve E_2, as E_2 is more sensitive to the disorder than E_1. Nevertheless, we can derive a similar threshold value of $\sim 5.9 \times 10^{14}$ cm^{-2}, from the E_1 plot. Our estimated threshold fluence for amorphization is in excellent agreement with results obtained from another technique.[43] The decrease of the amplitude of ε_2 with increasing fluence is interpreted as the decreasing probability of finding a crystallite with the minimum size required to produce a recognizable crystalline response. Following the approach of Aspnes *et al.*,[44] the slope in Fig. 4 refers to the projected area of excitation of core electrons and we find an area of $\sim (10 \text{ Å})^2$ perpendicular to the beam direction. This indicates that up to a minimum grain size of ~ 10 Å crystalline effect in the spectra may be retained to some extent and below which complete overlapping of the amorphous pockets leads to smearing out of the spectral features. In general, the definition of minimum grain sizes that can be detected in different experiments depends on the response being measured. From oscillator fitting of the spectral linewidth a similar grain size was estimated, as will be shown in the subsequent discussion. In the high fluence regime, a lower slope for $\Delta \varepsilon_2$ plot refers to a much lower grain size (<10 Å) and they are responsible for the small features in the ε_2 spectrum shown in Fig. 3. This implies that the dielectric spectra measured by ellipsometry offers a better resolution compared to many other techniques in estimating crystallite sizes contributing to optical excitations. It can be noted that the typical grain sizes encountered in deposited *a*-Si are usually smaller
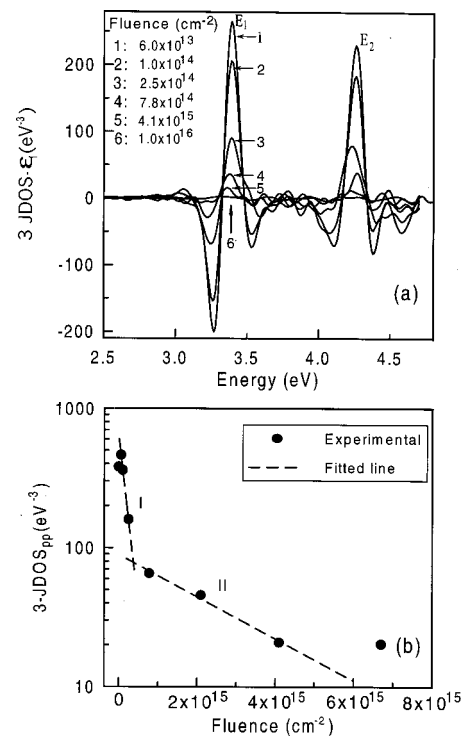
than the sizes obtained here and this causes a broad featureless spectrum in *a*-Si. In contrast, due to small but finite grain sizes in *i*-*a*-Si, small residual features remain in the dielectric spectra. Therefore, the differences in the dielectric spectra from differently prepared *a*-Si arise due to microstructural differences such as the presence of short-range order and a kind of paracrystalline state in *i*-*a*-Si. The occurrence of a sharp transition as shown in Fig. 4 cannot be understood using an amorphization model involving a minimum DPA. In the literature, the process of amorphization has been considered as a critical-point phenomena involving the cooperative behavior of damage accumulation and a collapse of the structure. From the estimation of the root mean square atomic displacement of the lattice sites, heavily damaged states were found to be far from equilibrium and at the *c*-*a* transition, the state was argued to be highly metastable.[2] Our results essentially support this model and the presence of a sharp transition refers to a first-order transition. These results indicate that the *i*-*a*-Si state is thermodynamically different from the defected crystalline state and a large heat of relaxation[45] can be understood in terms of the relaxation of the paracrystalline state towards the continuous random network.[19]

For a qualitative evaluation of the effect of disorder on the dielectric spectra, following the work of Aspnes *et al.*,[44] third joint density of states (3JDOS) derivatives were calculated numerically from the ε_1 spectrum and are shown in Fig. 5(a), for various fluences. For the fluences well below the amorphization threshold, the peak-to-peak height of the E_1 and E_2 peaks follows an exponential decay with increas-
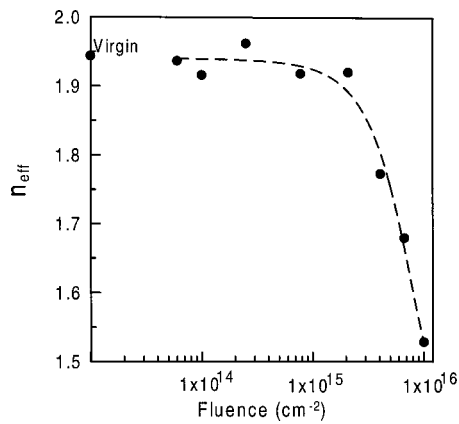
FIG. 6. The variation of the effective number of valence electrons (n_{eff}) per atom as a function of fluence evaluated at $E_{\text{max}} = 5.0$ eV. The dashed line is a guide to the eye.
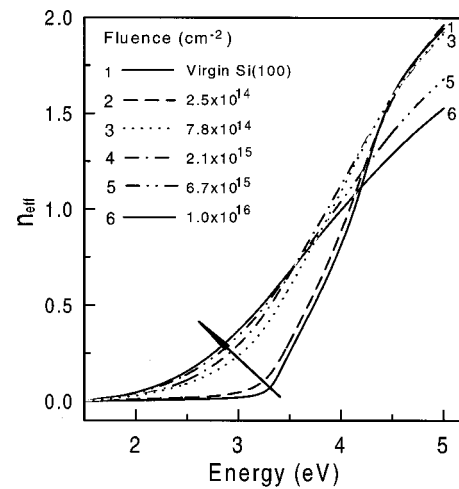

FIG. 7. The n_{eff} (per atom) as a function of the photon energy evaluated for various fluences. Arrow indicates the trend with increasing fluence.

ing fluence, as expected from Poisson statistics for damage buildup.[44] However, for higher fluences, the decay shows a different decay constant. Figure 5(b) shows the logarithm of 3JDOS peak-to-peak height as a function of fluence, which clearly exhibits two distinct slopes for regions I and II. The crossover point of two slopes refers to the threshold fluence for the crystalline to amorphous transition. In the low fluence regime (region I), from exponential dependence [$\sim \exp(-\alpha F)$, F is the fluence] of the 3JDOS peak-to-peak height, we estimate $\alpha = 55.8 \times 10^{-16}$ cm^2, which refers to a projected area of $\sim (90 \text{ Å})^2$ of the excitation on the plane perpendicular to the ion track. This value agrees well with the literature reports.

B. Moment calculations and band structure evolution

Here we evaluate various sum rules and moments shown in Eqs. (1)–(6), as these provide useful insight into disorder induced changes in various physical parameters. In particular, the moments provide the average properties of the electronic structure in the disordered material and they allow direct comparison between different materials in terms of their known physical parameters, such as dielectric constant, free carrier density, coordination number, bond length, etc. We use the $\varepsilon_2(E)$ spectra in the energy range 1.5–5.0 eV to calculate various moments and the macroscopic quantities defined in Eqs. (1)–(6). Figure 6 shows the variation of effective number of valence electrons per atom (n_{eff}, calculated for $E_{\text{max}} = 5.0$ eV) participating in the optical transitions as a function of fluence. It is seen that the n_{eff} does not change appreciably up to a fluence of $\sim 1 \times 10^{15}$ cm^{-2} above which it falls sharply with fluence. No appreciable difference in n_{eff} is observed for samples implanted with fluences 1×10^{16} and 1×10^{17} cm^{-2} indicating saturation in the carrier compensation by the process of ion damage. For the fluence above the amorphization threshold, we observe a continuous change in the n_{eff} indicating distinct changes in the band structure. Figure 7 shows the details of the energy response of n_{eff} for various fluences. It also displays distinct changes in n_{eff} spectra above the amorphization threshold. In particular, it can be seen that the low energy (around 3 eV) transitions contribute significantly to n_{eff} for heavily disordered

material compared to the c-Si and this is similar to the case of deposited a-Si.[46] In high-energy part, a decrease in n_{eff} is observed with increasing disorder. In c-Si, transitions between 1.1 and 3.4 eV are indirect, i.e., they take place between states of different k vector and only the simultaneous absorption or emission of a phonon allows for a weak absorption in that region. The lack of k conservation in a-Si makes these transitions quasi-allowed. From the harmonic oscillator fitting of the dielectric function, it is shown later that indeed the probability of the 3.4 eV transition increases with increasing disorder, indicating the loss of k conservation. The arrow in Fig. 7 indicates an increase in n_{eff} with fluence. The major changes in n_{eff} spectra can be understood on the basis of differences in the density of valence states and this also causes a small redshift in the maximum of ε_2 spectra of i-a-Si as shown in Table I.

In case of i-a-Si, it is usually believed that for fluences beyond the amorphization threshold no change in the microstructure occurs, except for an increase in the thickness of the amorphous layer with higher fluences. However, there has been a report on the nonuniformity in the damage profile in ion-damaged silicon, having a less damaged region near the surface compared to the bulk regions.[47] In the present case, the gradual change of various physical parameters can be understood if it is assumed that increasing fluences beyond the amorphization threshold cause continuous changes in the microstructure in the medium and thus the dielectric spectra evolve showing essential changes in various physical parameters as listed in Table I. In particular, we believe that with increasing fluence, the system evolves from medium-range order to short-range order and finally short-range order is reduced with very high fluence. In other words, the crystallite sizes diminish continuously and a complete overlap of the pockets of damaged regions would cause a broad spectrum in pure a-Si. However, the presence of small features (specifically for E_1 as shown in Fig. 3) essentially indicates that short-range order is not completely destroyed in such materials as compared to d-a-Si. Similar conclusions have been made by using electroreflectance measurements of i-a-Si[42] and more recently from fluctuation microscopy

TABLE I. Fluence dependence of effective dielectric constant ($\varepsilon_{0,\text{eff}}$), dispersion oscillator energy (E_0), average strength of the interband optical transition (E_d), nearest-neighbor coordination number (c), and position of $\varepsilon_{2\text{max}}$ (E_1) for 120 keV Ar$^+$ damaged Si.

Fluence (cm^{-2})	$\varepsilon_{0,\text{eff}}$	E_0 (eV)	E_d (eV)	Coordination number(c)	Position of $\varepsilon_{2\text{max}}$ (eV)
0	9.449	3.786	31.989	4.00	3.43
6.0×10^{13}	9.532	3.736	31.880	3.99	3.44
1.0×10^{14}	9.740	3.589	31.366	3.95	3.44
2.5×10^{14}	9.854	3.592	31.806	3.96	3.46
7.8×10^{14}	11.407	3.096	32.226	3.78	3.45
2.1×10^{15}	11.795	3.036	32.774	3.75	3.41
4.1×10^{15}	11.579	2.901	30.688	3.75	3.39
6.7×10^{15}	11.222	2.857	29.208	3.69	3.38
1.0×10^{16}	10.807	2.773	27.193	3.68	3.34
1.0×10^{17}	10.470	2.877	27.264	3.63	3.36
i-a-Si [a]	11.974	2.824	30.992	3.63	3.33
a-Si [b]	9.374	3.041	25.460	3.66	3.45

[a]See Ref. 26.
[b]See Ref. 37.

analysis.[19] From theoretical calculations on a-Si, it is understood that prominent features in the DOS and optical properties of a-Si can be understood in terms of a short-range disorder model.[48] From a structural point of view, amorphous systems are often characterized as crystalline material in which long-range order is lost. However, theoretical studies on complex crystalline models indicate that long range-disorder effects are of secondary importance in optical spectra and it is the short range-disorder which is essential to reproduce the broad featureless spectra of a-Si. With deviations in bond angles and bond length, and with odd membered ring of bonds, it is possible to account for both features of DOS and optical properties. Hence, essential difference between i-a-Si and d-a-Si lie in degree of short-range order in the structure.

In Fig. 8 we show the calculated Penn gap as a function of fluence and it shows a systemic decrease with increasing fluence. It can be noted that a drastic change in the Penn gap occurs once the amorphization threshold fluence is achieved and below this threshold, no substantial change in gap occurs. This decrease in the Penn gap indicates that average separation between bonding and antibonding states decreases with increasing fluence. This can be understood in the frame-work of the creation of band tail states due to disorder in crystalline structure, which in turn reduce the effective gap between the valence and conduction bands. Furthermore, a decrease in the Penn gap implies an average reduction in bond strength and decreased covalency.[32] The covalent bonds in c-Si are easily broken by the energetic ions in the process of irradiation and due to the incomplete reconstruction of bonds and bond switching, an average reduction in covalent bonds with increasing disorder is anticipated. In the process of disorder a large change in bond angle and bond length is usually encountered, as is known for an a-Si structure. From an empirical relationship between the Penn gap and bondlength,[49] ($\eta\omega_g \propto r^{-2.5}$, where r is the bond length) we estimate the change in bond length with increasing disorder and this is plotted in Fig. 8. This shows an increase of $\sim 8\%$ in bond length for the highest fluence implanted sample in comparison to c-Si assuming a bond length of 2.352 Å. This value is relatively large compared to the value known for evaporated a-Si which shows a difference of $\sim 2\%$. However, properties of a-Si prepared by conventional methods depend strongly on preparation conditions. The presence of voids in a-Si may regulate any large change of bond length that gives rise to a relatively smaller change with a larger number of voids.

On the other hand, in implanted Si the change in bond length may be dictated primarily by the atomic mass of the implanted ion species and the absence of the void will allow larger stretching of the bonds. It may be noted that in the present work, the moment calculations were performed up to the energy of 5.0 eV that may be inadequate to provide sufficient accuracy for the exact comparison of parameters obtained from different measurements. A more exact comparison would be possible if the dielectric function is evaluated to a higher energy range. From the calculated Penn gap, an estimate of the change in the coordination number with increasing disorder can be made. From the known square root dependence of the coordination number on the Penn gap, we estimate the coordination number (c) to be ~ 3.63 for the sample implanted with the highest fluence, assuming c
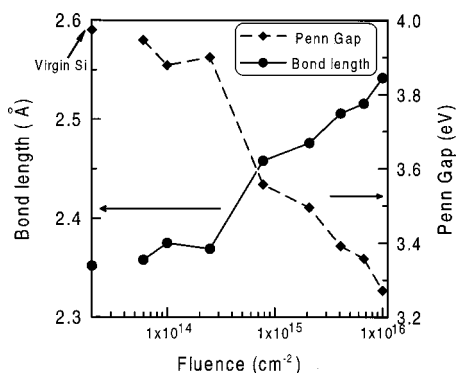

FIG. 8. Calculated Penn gap and bond length variation as a function of fluence. The arrows indicate the corresponding Y axes used for respective curves.

=4.0 for crystalline Si. This value is close to the values obtained from other experiments. For example, the RDF evaluation showed a $c \sim 3.79$ in as-implanted i-a-Si samples.[16] In our case, a continuous change in these physical parameters with fluence above the threshold indicates the gradual evolution of the microstructure and the band structure. Though in many models a-Si is assumed to have the same coordination number as c-Si, from theoretical calculations it has been recently found to have a coordination number less than 4,[50] in contrast to the majority of the theoretical predictions which derive values greater than 4. Nevertheless, experimentally obtained values are always less than 4 and that is accounted for the reduced density of a-Si compared to c-Si.[16]

Various other physical parameters defined in Sec. III are evaluated and presented in Table I, to enable proper comparison of the systematic changes with fluence. It can be seen from the table that with increasing fluence, E_0 and E_d decrease substantially at fluences above the amorphization threshold. Below the amorphization threshold, no substantial change in these parameters is observed indicating the insensitivity of these parameters to the presence of point defects, despite a high concentration being present in the damaged Si. Above the threshold fluence, due to gradual reduction of crystalline size, marked influence on the parameters is observed and it indicates that these parameters are extremely sensitive to the microstructure of the material.[49] Similar features are observed for a change in the effective dielectric constant ($\varepsilon_{0,\text{eff}}$). Above the amorphization threshold, a marked increase in $\varepsilon_{0,\text{eff}}$ is observed with respect to the virgin sample and for maximum fluence it reduces slightly from its maximum value of 11.8 corresponding to a fluence of 2.1×10^{15} cm^{-2}. On the other hand, a monotonic decrease of E_0 and E_d is observed with increasing disorder and it is found to saturate for very high fluence (1×10^{17} cm^{-2}). Wemple and DiDomenico relate the dispersion energy E_d to be a direct measure of the optical conductivity σ and consequently to an interband oscillator strength parameter.[33] Therefore, a decrease in E_d with increasing disorder refers to a reduction in the optical conductivity, which is consistent with the observed reduction in n_{eff}. Normalized E_d or σ has been defined to be a universal constant in a wide range of covalent and ionic crystal. Hence, the observed changes in E_d in the present case points to the corresponding changes in the nearest-neighbor coordination number, effective number of valence electrons, and anion valency.

C. Lorentz oscillator fitting and band structure evolution

With a view to provide a phenomenological description of the disordered material produced by ion implantation, we use a set of harmonic oscillators to fit the measured pseudodielectric functions. This spectral representation provides an analytical description of $\varepsilon(E)$ as a function of fluence and has been utilized in the past in analyzing implantation damage in Si[10] and GaAs.[34] We specifically focus on the variation of the amplitude and linewidth of each oscillator with increasing fluence, because the critical points broaden and weaken differently as the disorder destroys the momen-
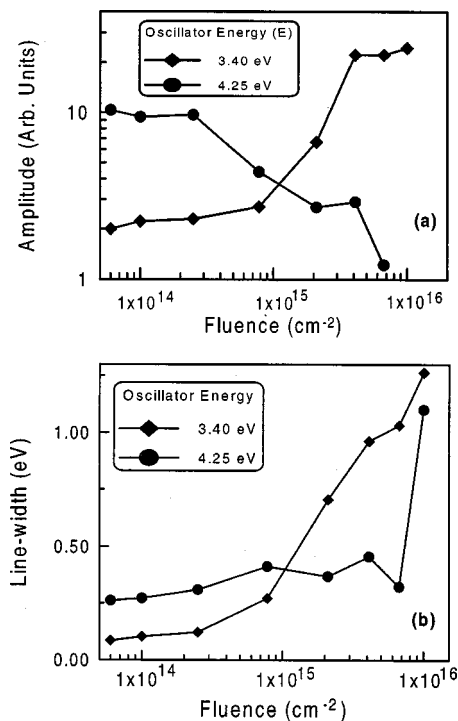

FIG. 9. (a) Oscillator amplitude, and (b) linewidth variation with fluence for the two major transitions at 3.40 eV and 4.25 eV. A set of six Lorentz oscillators was assumed for fitting the complex dielectric function of ion-damaged silicon.

tum conservation. We have found that a minimum of six oscillators is required in this spectral region to fit the dielectric function of Si disordered to varying degrees. All 18 parameters A_i, E_i, Γ_i [defined in Eq. (7)] for fitting were obtained by a linear regression analysis using a simplex multiparameter algorithm for the simultaneous fitting of the real and imaginary part of the complex dielectric spectra. The quality of the fit was assessed through a check in the standard deviation which yielded a value of $\sim 1\%-3\%$. The convergence was good, because the oscillators are weakly correlated. A first round of fitting on all samples indicated the approximate invariance of E_i for different samples. The $\varepsilon(E)$ spectra of the implanted samples were fitted using same set of six oscillators except that the A_i and Γ_i were considered as adjustable parameters. The oscillator energies obtained for c-Si ($E_i = 3.40$, 3.60, 3.90, 4.25, 4.81, and 5.53 eV) were treated as constant in each case. The oscillators at 3.40 and 4.25 eV are responsible for the major structures E_1 and E_2 respectively, which show up in $\varepsilon_2(E)$ spectra shown in Fig. 3. The oscillator at 5.55 eV also contributes to the broad tail of the spectra and is related to M_3 critical point at the L symmetry point in the Brillouin zone.[51] The other oscillators with intermediate energies were necessary to fit rather deep minimum and the slope change in ε_2 spectra. A close look at the fitted parameters shows that the linewidth (Γ_i) increases with fluence for all the transitions (E_i), whereas amplitude (A_i) decreases with fluence, except for the case of 3.40 eV transition. Figure 9 shows the amplitude and linewidth variation as a function of fluence for the two major transitions E_1 (3.40 eV) and E_2 (4.25 eV). It shows that amplitude of E_1 transition increases with fluence, while

for E_2 transition it decreases with fluence [see Fig. 9(a)]. However, the linewidth increases with fluence for both the transitions as expected due to interaction with phonons and other scatterers. Figure 9 shows that extent of change in the amplitude and linewidth is very large in the case of the 3.40 eV transition, compared to the 4.25 eV transition. Hence, the low energy part of the band structure is most affected by the induced disorder in Si. Though a reduction in the oscillator amplitude with increased disorder can be understood on the basis of band flattening, increased amplitude in the case of the 3.40 eV transition refers to a modification in the band structure such that an enhanced probability of transition occurs at ~3.40 eV. This can be caused by reducing the effective separation between the valence band and conduction band edges. This is consistent with an increase in n_{eff} at lower energy for higher fluence shown in Fig. 7. These analyses demonstrate that by introducing controlled disorder, it is possible to increase the probability of certain optical transitions with a small broadening in the linewidth. Our fitting also shows that the 4.25 eV linewidth does not increase rapidly with fluence compared to the 3.40 eV transition. From the linewidth variation, it is possible to correlate the corresponding changes in the crystallite size using the approach used in by Feng and Zallen.[52] This approach is based on the fact that the spectral linewidth is related to the lifetime of the carriers. It is assumed that in the disordered structure, the k vector broadening results from the finite crystallite size and the corresponding reduction of the carrier lifetime due to boundary scattering. From the reciprocal dependence of crystallite size with linewidth, an estimate of the crystallite sizes with different fluences shows that amorphization threshold corresponds to a grain size ~9 Å. These small crystallites in implanted amorphous Si are responsible for the peak-like features in the imaginary part of the dielectric spectrum shown in Fig. 3. Therefore, a microcrystalline model is more appropriate than the continuous random network model for a proper description of the structure and optical properties of pure amorphous Si.

V. CONCLUSIONS

Crystalline to amorphous transition and subsequent microstructural evolution of ion-damaged Si has been studied by spectroscopic ellipsometry. In the evaluation of the optical spectra, the contribution of a surface oxide layer was separated from the measured dielectric spectra by using a multilayer model with an effective medium approximation. The difference spectra as a function of fluence exhibit a distinct transition from the crystalline to amorphous phase and the threshold fluence derived for this transition matches very well with the literature reports. Fluence dependence of various moments of ε_2 spectra shows a systematic change in various physical parameters such as $\varepsilon_{0,eff}$, n_{eff}, E_0, E_d, Penn gap, bond length, and coordination number. Beyond the amorphization threshold these parameters change drastically and a continuous evolution of the system occurs with higher fluences. These parameters are found to be least sensitive to point defects present in damaged Si. Major changes in the optical properties and electronic structure for high fluences have been correlated with the reduction in crystallite size and band-structure evolution. It is also shown that the dielectric function obtained by ellipsometric measurements is well represented by a set of six classical Lorentz oscillators. With increasing fluence, the oscillator amplitude diminishes and spectral linewidth increases, except for the 3.3 eV transition which shows increasing amplitude with fluence. These results are explained by taking into account the loss of medium- and short-range order and flattening of the band structure with increasing fluence.

[1] O. W. Holland and S. J. Pennycook, Appl. Phys. Lett. **55**, 2503 (1989).
[2] G. A. Bai and M.-A. Nicolet, J. Appl. Phys. **70**, 649 (1991).
[3] S. U. Campisano, S. Coffa, V. Raineri, F. Priolo, and E. Rimini, Nucl. Instrum. Methods Phys. Res. B **80/81**, 514 (1993).
[4] T. Diaz de la Rubia and G. H. Gilmer, Phys. Rev. Lett. **74**, 2507 (1995).
[5] T. Motooka, S. Hurada, and M. Ishimaru, Phys. Rev. Lett. **78**, 2080 (1997).
[6] J. A. Davies, J. Denhartog, L. Eriksson, and J. W. Mayer, Can. J. Phys. **45**, 4053 (1967).
[7] J. Narayan, D. Fathy, O. S. Oen, and O. W. Holland, J. Vac. Sci. Technol. A **2**, 1303 (1984).
[8] K. Laaziri, S. Kycia, S. Roorda, M. Chicoine, J. L. Robertson, J. Wang, and S. C. Moss, Phys. Rev. B **60**, 13 520 (1999).
[9] T. Motooka and O. W. Holland, Appl. Phys. Lett. **58**, 2360 (1991).
[10] A. Borghesi, A. Piaggi, A. Stella, G. Guizzetti, D. Bisero, and G. Queirolo, J. Appl. Phys. **67**, 7045 (1990).
[11] N. V. Nguyen, K. Vedam, and J. Narayan, J. Appl. Phys. **67**, 599 (1990); S. Boultadakis, S. Logothetidis, and S. Ves, *ibid.* **72**, 3648 (1992).
[12] J. T. Lue and S. Y. Shaw, J. Appl. Phys. **53**, 5617 (1982).
[13] M. O. Ruault, J. Chaumont, and H. Bernas, Nucl. Instrum. Methods Phys. Res. **209/210**, 351 (1983).
[14] L. J. Lewis and R. M. Nieminen, Phys. Rev. B **54**, 1459 (1996).
[15] J. S. Custer, M. O. Thompson, D. C. Jacobson, J. M. Poate, S. Roorda, W. C. Sinke, and F. Spaepen, Appl. Phys. Lett. **64**, 437 (1994).
[16] K. Laaziri, S. Kycia, S. Roorda, M. Chicoine, J. L. Robertson, J. Wang, and S. C. Moss, Phys. Rev. Lett. **82**, 3460 (1999).
[17] S. C. Moss and J. F. Graczy, Phys. Rev. Lett. **23**, 1167 (1969).
[18] R. Car and M. Parrinello, Phys. Rev. Lett. **60**, 204 (1988).
[19] J. M. Gibson, J.-Y. Cheng, P. Voyles, M. M. J. Treacy, and D. C. Jacobson, Mater. Res. Soc. Symp. Proc. **540**, 27 (1999).
[20] J. M. Gibson and M. M. J. Treacy, Phys. Rev. Lett. **78**, 1074 (1997).
[21] D. L. Wiliamson, S. Roorda, M. Chicoine, R. Tabti, P. A. Stolk, S. Acco, and F. W. Saris, Appl. Phys. Lett. **67**, 226 (1995).
[22] L. Sealy, R. C. Barklie, K. J. Reeson, W. L. Brown, and D. C. Jacobson, Nucl. Instrum. Methods Phys. Res. B **62**, 384 (1992).
[23] D. E. Aspnes, in *Handbook of Optical Constant of Solid*, edited by E. B. Palik (Academic, New York, 1985).
[24] G. E. Jellison, Opt. Mater. **1**, 41 (1992).
[25] V. Grasso, G. Mondio, G. Saitta, S. U. Campisano, G. Foti, and E. Rimini, Appl. Phys. Lett. **33**, 632 (1978).
[26] M. Fried, T. Lohner, W. A. M. Aarnink, L. J. Hanekamp, and A. Van Silfout, J. Appl. Phys. **71**, 2835 (1992).
[27] W. Fukarek and J. R. Kaschny, J. Appl. Phys. **86**, 4160 (1999).
[28] M. Fried, T. Lohner, W. A. M. Aarnink, L. J. Hanekamp, and A. Van Silfhout, J. Appl. Phys. **71**, 5260 (1992).
[29] D. E. Aspnes and A. A. Studana, Phys. Rev. B **27**, 985 (1983).
[30] L. Ley, in *The Physics of Hydrogenated Amorphous Silicon II*, edited by J. D. Joannopolos and G. Lucovsky (Springer, Berlin, 1984), p. 61.
[31] D. R. Penn, Phys. Rev. **128**, 2093 (1962).
[32] J. C. Phillips and J. A. Van Vechten, Phys. Rev. Lett. **22**, 705 (1969).
[33] S. H. Wemple and M. DiDomenico, Jr., Phys. Rev. Lett. **23**, 1156 (1969).
[34] M. Erman, J. B. Theeten, P. Chambon, S. M. Kelso, and D. E. Aspnes, J. Appl. Phys. **56**, 2664 (1984).
[35] T. Lohner, N. Q. Khanh, P. Petrik, M. Fried, E. Kotai, and J. Gyulai, Mater. Sci. Forum **248–249**, 229 (1997).
[36] T. Lohner, M. Fried, N. Q. Khanh, P. Petric, H. Wormester, and M. A. El-Sherbiny, Nucl. Instrum. Methods Phys. Res. B **147**, 90 (1999).
[37] D. T. Pierce and W. E. Spicer, Phys. Rev. B **5**, 3017 (1972).
[38] S. Lee, S. Y. Kim, and S. Oh, Jpn. J. Appl. Phys., Part 1 **35**, 5929 (1996).

[39] S. Adachi, T. Matsumura, and T. Suzuki, Jpn. J. Appl. Phys., Part 1 **33**, 1931 (1994).

[40] J. F. Ziegler, J. P. Biersack, and U. Littmark, *The Stopping of Ion Range in Solids* (Pergamon, New York, 1985).

[41] X. F. He, R. R. Jiang, R. X. Chen, and D. Mo, J. Appl. Phys. **66**, 5261 (1989).

[42] M. Geddo, D. Maghini, and A. Stella, Solid State Commun. **58**, 483 (1986).

[43] A. Claveri, C. Vieu, J. Faure, and J. Beauvillain, J. Appl. Phys. **64**, 4415 (1988).

[44] D. E. Aspnes, S. M. Kelso, C. G. Olson, and D. Y. Lynch, Phys. Rev. Lett. **48**, 1863 (1982).

[45] S. Roorda, S. Doorn, W. C. Sinke, P. M. L. O. Scholte, and E. Van Loenen, Phys. Rev. Lett. **62**, 1880 (1989).

[46] S. Logothetidis and G. Kiriakidis, J. Appl. Phys. **64**, 2389 (1988).

[47] P. X. Zhang, I. V. Michell, B. Y. Tong, P. J. Schultz, and D. J. Lockwood, Phys. Rev. B **50**, 17 080 (1994).

[48] J. D. Joannopoulos and M. L. Cohen, Solid State Phys. **31**, 71 (1976).

[49] G. A. N. Connel, in *Amorphous Silicon*, edited by M. H. Broadsky (Springer, Berlin, 1979).

[50] N. C. Cooper, C. M. Goringe, and D. R. McKenzie, Comput. Mater. Sci. **17**, 1 (2000).

[51] M. L. Cohen and J. R. Chelikowsky, *Electronic Structure and Optical Properties of Semiconductors* (Springer, Berlin, 1988).

[52] G. F. Feng and R. Zallen, Phys. Rev. B **40**, 1064 (1989).